Hydrostatic deformation potentials of narrow-gap HgCdTe

Maria Szoła [1,*] Yurii Ivonyak [2] Jacek Przybytek [2] Nikolai Mikhailov,[3,4] Sergey Dvoretsky [3,4]
Frédéric Teppe [2,1] and Wojciech Knap[2,1]

[1]*Laboratoire Charles Coulomb (L2C), UMR 5221 CNRS-Université de Montpellier, F-34095 Montpellier, France*
[2]*CENTERA Laboratories, Institute of High Pressure Physics, Polish Academy of Sciences, PL-01-142 Warsaw, Poland*
[3]*A.V. Rzhanov Institute of Semiconductor Physics, Siberian Branch of the Russian Academy of Sciences, 630090 Novosibirsk, Russia*
[4]*Novosibirsk State University, 630090 Novosibirsk, Russia*

Close to the semimetal-to-semiconductor topological phase transition, the band structure of HgCdTe is represented by massive Kane fermions that, in a semirelativistic approach, are characterized by two parameters: rest mass and velocity. Using terahertz magneto-optical spectroscopy, we explore the band structure evolution of HgCdTe films with hydrostatic pressure in the vicinity of the band-gap collapse. By analyzing the energies of interband optical transitions as a function of magnetic field, we have determined the rest mass of Kane fermions at different hydrostatic pressures. The pressure dependence of the rest mass allows us to obtain the hydrostatic deformation potential $a_c - a_v$ at low temperature, where a_c and a_v are the deformation potentials of the conduction and valence bands, respectively.

I. INTRODUCTION

Among numerous narrow-gap materials, $Hg_{1-x}Cd_xTe$ alloys have been widely exploited in the field of terahertz photodetectors [1]. The technological progress achieved in the last two decades in pseudomorphic growth of homogeneous thin films and HgCdTe-based heterostructures [2] makes them also attractive for terahertz sensors [3,4] and lasers [5–7]. The specific advantages of $Hg_{1-x}Cd_xTe$ are the direct band gap, ability to obtain both low and high carrier concentrations, high mobility of electrons, low dielectric constant, and wide band-gap tunability.

The band structure of $Hg_{1-x}Cd_xTe$ can be tuned from inverted-band semimetal of HgTe to conventional semiconductor of CdTe by adjusting the Cd composition x, or externally, by changing temperature [8,9]. For instance, the band inversion between the Γ_6 and Γ_8 bands in $Hg_{1-x}Cd_xTe$ occurs at $x \lesssim x_c$, where x_c is a temperature-dependent parameter ($x_c \simeq 0.165$ at 2 K and $x_c \simeq 0.155$ at 77 K [8]). In this sense, semimetallic $Hg_{1-x}Cd_xTe$ is also called "semiconductor with negative band gap" E_g assuming the energy difference between the Γ_6 and Γ_8 bands. The possibility of band inversion yields various topological states of matter in HgCdTe bulk films [10–14] and HgTe/HgCdTe quantum wells [15–18]. Interestingly, the temperature-dependent band gap in HgCdTe alloys provides an additional opportunity for temperature tuning of topological phase transitions in HgCdTe-based heterostructures [19–21].

The band structure of these three-dimensional (3D) and two-dimensional systems is significantly affected by applied or intrinsic strain characterized by deformation potentials of the bulk constituents. For instance, the uniaxial strain defined by the shear deformation potentials b and d splits the Γ_8 band at the Γ point of the Brillouin zone and transforms semimetallic HgCdTe bulk films either into a 3D topological insulator [10,11,22] or into a 3D Dirac/Weyl semimetal [12,13]. In contrast, the hydrostatic deformation potentials a_c and a_v describe the evolution of the Γ_6 and Γ_8 bands, respectively, under applied strain. Although the values of a_c and a_v cannot be directly determined experimentally, their difference, $a_c - a_v$, however, can be extracted from the hydrostatic pressure dependence of the direct band gap $E_g(P)$ or $\partial E_g / \partial P$.

A large number of experimental investigations of $E_g(P)$ in $Hg_{1-x}Cd_xTe$ have been reported up to now [23–36]. They have been performed by means of transport measurements, optical absorption, reflectivity, and photoluminescence in conjunction with theoretical calculations. The experimental values of $\partial E_g / \partial P$ obtained by different authors are summarized in Table I. One can see that the scatter of the values is very large. The reasons for such a large scatter can be attributed to differences in experimental techniques, often leading to very cumbersome parameters extraction. For instance, to extract $\partial E_g / \partial P$ from transport data, one has to use the models containing a certain number of third-party parameters, whose values are not exactly known and differ from work to work [30–35]. In this sense, the most reliable data can be obtained from the optical absorption, reflectivity, or photoluminescence, allowing measuring E_g most directly.

Currently, the most self-consistent values of $\partial E_g / \partial P$ and deformation potentials of $Hg_{1-x}Cd_xTe$ were determined by linear interpolation between the values of CdTe [23–26] and the values of HgTe obtained by Latussek *et al.* [36]. The latter were extracted from optical absorption of HgTe/$Cd_{0.7}Hg_{0.3}$Te superlattices on the basis of band structure calculations within sophisticated numerical band structure calculations. Although

TABLE I. Pressure coefficients of the direct energy gap E_g for Hg$_{1-x}$Cd$_x$Te bulk crystals obtained by transport, optical absorption, reflectivity, and photoluminescence (PL) techniques.

	$\partial E_g/\partial P$ (meV/kbar)	T (K)	Method
$x = 1$	7.9 ± 0.2	300	Reflectivity [23]
	8.0		PL [24]
	8.3		Absorption [25]
	8.4		Absorption [26]
	7.9 ± 0.2	77	PL [27]
	6.5 ± 0.2	2	PL [28]
$x = 0.7$	8.7	300	Absorption [29]
$x < 0.3$	8.7	> 77	Transport [30]
$x = 0.27$	10.0	4.2	Transport [31]
$x = 0.164$	8.0	300	Transport [32]
$x = 0.15$	7.0	77	Transport [33]
	3.0		Transport [34]
$x = 0$	10.4 ± 0.6	300	Transport [35]
	8.72 ± 0.25^a		Absorption [36]

^{a}Analysis of intersubband transitions in HgTe/Hg$_{0.3}$Cd$_{0.7}$Te superlattices assuming $\partial E_g/\partial P = 7.9$–8.4 meV/kbar for bulk CdTe [23–26].

TABLE II. Parameters of Hg$_{1-x}$Cd$_x$Te samples studied in this work and the values of deformation potential $(a_c - a_v)$ at 2 K determined from terahertz magneto-optical spectroscopy (see Sec IV).

Sample	x	$(a_c - a_v)$ (eV)
A	0.152	-2.87 ± 0.09
B	0.165	-2.86 ± 0.11
C	0.172	-2.83 ± 0.12

the deformation potentials $a_c - a_v$ of CdTe [23–26] and HgTe [36] were obtained at *room temperatures* only, they are widely used for theoretical description of low-temperature investigations of HgTe/HgCdTe quantum wells [11,13,16,20,21].

In this work, we address the question of the *low-temperature* band-gap evolution of Hg$_{1-x}$Cd$_x$Te films with hydrostatic pressure in the vicinity of the band-gap collapse, i.e., for $0.155 \leqslant x \leqslant 0.175$. By using terahertz magneto-optical spectroscopy, we directly determine the band-gap values at 2 K at different hydrostatic pressure avoiding sophisticated band structure calculations required for analyzing HgTe/HgCdTe superlattices [36]. Note that terahertz magneto-optical spectroscopy of HgCdTe allows one to probe both positive and negative E_g values [8] corresponding to the semiconductor and semimetallic films, respectively. By using linear extrapolation between our values and those of Dunstan *et al.* [28] for CdTe at 2 K, we determine the deformation potential $a_c - a_v$ at low temperatures for any values of x.

In many multilayer systems the substrate plays an important role—especially in the pressure/strain-dependent measurements. Recently, experiments have been performed on samples with etched substrate. No differences have been observed between hydrostatic pressure results obtained on the standard and substrate etched samples. This peculiar behavior is attributed to a specific layer sequence of the samples in which most probably a highly dislocated CdTe buffer layer leads to relaxation of the influence of the substrate on the HgCdTe layer in the pressure experiments [37].

II. EXPERIMENTAL DETAILS

The Hg$_{1-x}$Cd$_x$Te alloys layer was grown on SI (013)GaAs, including ZnTe and CdTe buffer layers by molecular beam epitaxy. The growth was carried out in a special ultrahigh-vacuum multichamber molecular beam epitaxy set "Ob-M," which allows for the growth of very high-quality HgCdTe

crystals with monitoring by reflection high-energy electron diffraction and single wavelength ultrafast ellipsometry (0.5 nm) *in situ* [38]. The Cd concentration was chosen in the range near the critical value $x_c \simeq 0.165$ corresponding to the semimetal-to-semiconductor topological phase transition at 2 K [8]. We performed magneto-optical studies on three (013)-oriented Hg$_{1-x}$Cd$_x$Te samples with $x = 0.155$, 0.165, and 0.175 calculated from measured transmission spectra at 300 K by a developed method for HgCdTe absorber layers between two graded wide gap layers at boundaries. The Hg$_{1-x}$Cd$_x$Te layers were sufficiently thick (≈ 3.2 μm) to be considered as 3D materials and thin enough to be transparent in the far-infrared spectral range. Parameters of the sample are listed in Table II.

The magneto-optical measurements in magnetic fields up to 5 T were carried out at $T = 2$ K in a beryllium-bronze clamp cell with liquid (1:1 kerosene with transformer oil) as a pressure transmitting medium. The pressure cell was custom-made to allow simultaneous transport and optical measurements. The scheme of the pressure cell is given in Ref. [39]. The cell was equipped with electrical wiring for transport measurements and an n-InSb pressure gauge used to measure pressure. We have used a Unipress [40] standard heavily doped n-InSb crystal calibrated at room and liquid-nitrogen temperatures. The calibration of the pressure gauge has been corrected by $<3\%$ correction resulting from the temperature difference between 77 K and liquid-helium temperature. The initial pressure was applied at room temperature, and then the cell was inserted into the cryostat with a superconducting coil. After cooling to 2 K, the pressure in the cell significantly decreased to the value at which the measurements were performed. As a radiation source, we used the five lines of a far-infrared CO$_2$ laser 4.3 THz (70.6 μm, 17.6 meV), 3.1 THz (96.5 μm, 12.9 meV), 2.5 THz (118.8 μm, 10.4 meV), 1.8 THz (163.0 μm, 7.6 meV), and 1.6 THz (186.0 μm, 6.7 meV). For the lower-energy range, we utilized a backward wave oscillator and Virginia diodes source operating at 0.9 THz (334.6 μm, 3.7 meV) and 0.7 THz (454 μm, 2.7 meV), respectively. The radiation transmitted through the pressure cell was detected by a carbon bolometer (thinned Allen-Bradley carbon resistor). Spectra were normalized by the power of the laser, which was monitored at all times.

Figure 1 presents the typical magnetotransmission spectra of sample A measured at different frequencies of incident light and hydrostatic pressures. The spectra for other samples are given in the Supplemental Material [39]. All the spectra contain up to four absorption lines observed at all pressure values, identified as various Landau-level transitions. Following the
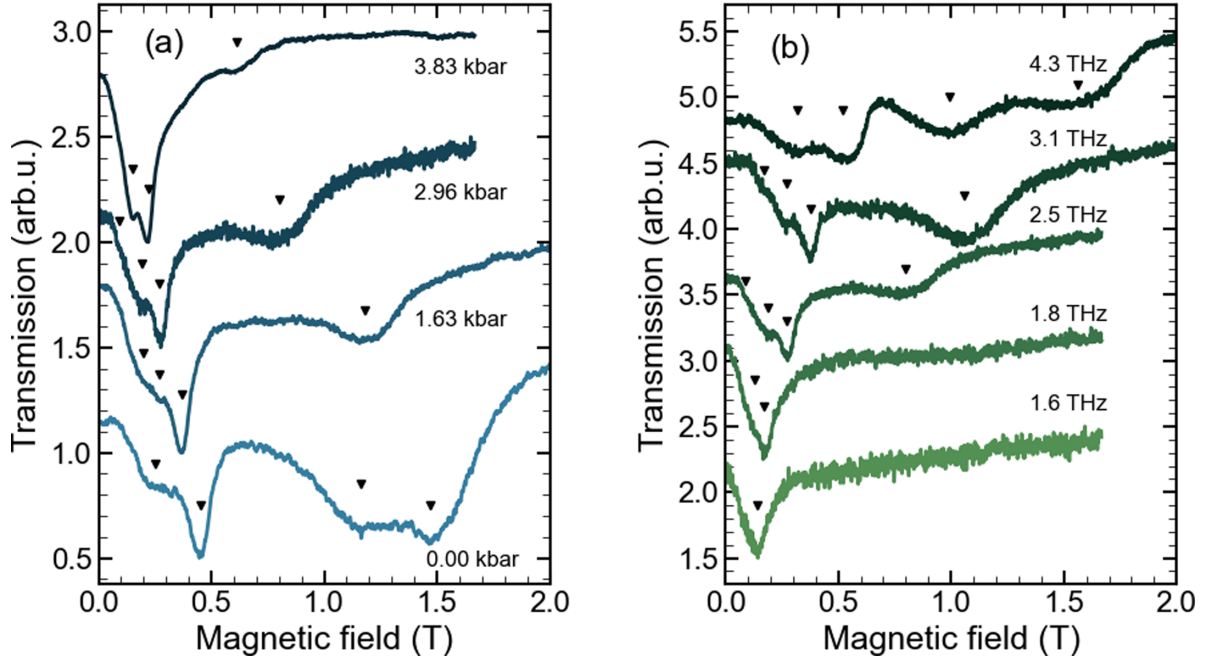
FIG. 1. (a) Magnetotransmission spectra of sample A measured at four hydrostatic pressures: $P = 0$ kbar, $P = 1.63$ kbar, $P = 2.96$ kbar, and $P = 3.83$ kbar, at the frequency of 2.5 THz. (b) Magnetotransmission spectra of sample A measured at different frequencies of incident light measured at $P = 2.96$ kbar. The magnetic fields corresponding to Landau-level transitions observed at a given energy of the incident radiation are marked by black triangles.

evolution of resonant energies of the absorption lines with the magnetic field, we can further extract the band gap at a given hydrostatic pressure.

III. LANDAU-LEVEL TRANSITIONS

To describe Landau-level (LL) transitions in $Hg_{1-x}Cd_xTe$ with x close to x_c, one can employ a simplified Kane model [8]. The latter takes into account linear $\mathbf{k} \cdot \mathbf{p}$ interaction between the Γ_6 and Γ_8 bands while neglecting the influence of the split-off Γ_7 band. Although the corresponding 6×6 Hamiltonian formally describes the dispersion of relativistic 3D particles, it cannot be reduced to the Dirac Hamiltonian due to unavoided hybridization in the two Γ_8 bands [41]. Thus, the term "Kane fermion" was invoked for the particles, whose Hamiltonian describes the band structure of HgCdTe in the vicinity of topological phase transition [42].

The simplified 6×6 Hamiltonian has three double-degenerate eigenvalues, which can be represented in the form [8]

$$E_\xi(p) = \xi^2 \tilde{m}\tilde{c}^2 + (-1)^{1-\theta(\tilde{m})}\xi\sqrt{\tilde{m}^2\tilde{c}^4 + p^2\tilde{c}^2}, \qquad (1)$$

where p is an absolute momentum value and $\theta(x)$ is a Heaviside step function, which equals to 1 for $x \geqslant 0$ and to 0 if x is negative. The first eigenvalue with $\xi = 0$ corresponds to the heavy-hole Γ_8 band, which is dispersionless in the linear approximation. The two other eigenvalues describe the electron Γ_6 ($\xi = +1$) and light-hole Γ_8 ($\xi = -1$) conical bands separated by $E_g = 2\tilde{m}\tilde{c}^2$, where $\tilde{m}$ and $\tilde{c}$ represent the rest mass and asymptotic velocity of Kane fermions [8], respectively.

The rest-mass parameter $\tilde{m}$ in Eq. (1) describes the semimetal-to-semiconductor topological phase transition in HgCdTe. If $\tilde{m}$ is positive, the crystal is a conventional

narrow-gap semiconductor with the s-type Γ_6 band lying above the p-type Γ_8 bands. On the other hand, the negative values of $\tilde{m}$ correspond to the band inversion, i.e., the Γ_6 band lies below the Γ_8 bands. As the two Γ_8 bands always touch each other at the Γ point of the Brillouin zone, the HgCdTe crystal is a semimetal at $\tilde{m} < 0$.

In the presence of a magnetic field, the energy dispersion of Kane fermions transforms into Landau levels with the energies [8]

$$E_{\xi,n,\sigma}(p_z) = \xi^2 \tilde{m}\tilde{c}^2 + (-1)^{1-\theta(\tilde{m})}$$

$$\times \xi\sqrt{\tilde{m}^2\tilde{c}^4 + \frac{e\hbar\tilde{c}^2 B}{2}(4n - 2 + \sigma) + \tilde{c}^2 p_z^2}, \quad (2)$$

where p_z is a momentum projection onto the direction of the magnetic field and n is the LL index, for which values depend on ξ. For $\xi = \pm 1$, n runs over positive integers $n = 1, 2, \ldots$, while for the zero-energy heavy-hole band ($\xi = 0$), n runs over all non-negative integers, except 1: $n = 0, 2, 3 \ldots$. The quantum number σ accounts for the Kramers' degeneracy lifted by the magnetic field $\mathbf{B} = (0, 0, B)$. The magneto-optical response is determined by electric-dipole selection rules: $\Delta n = n \pm 1$ with "$\pm$" corresponding to the two circular polarizations, $\Delta p_z = 0$, $\Delta \sigma = 0$, and no restriction on changing of ξ.

As seen from Eq. (2), it contains only two parameters $\tilde{m}$ and $\tilde{c}$, for which values can be extracted from the field evolution of multiple LL transitions observed in magnetotransmission spectra. Interestingly, the analysis of LL transitions based on Eq. (2) gives not only the absolute value of $\tilde{m}$ but also its sign [8]. The latter allows probing of the semimetal-to-semiconductor topological phase transition and determination E_g for semimetallic HgCdTe. The gap is
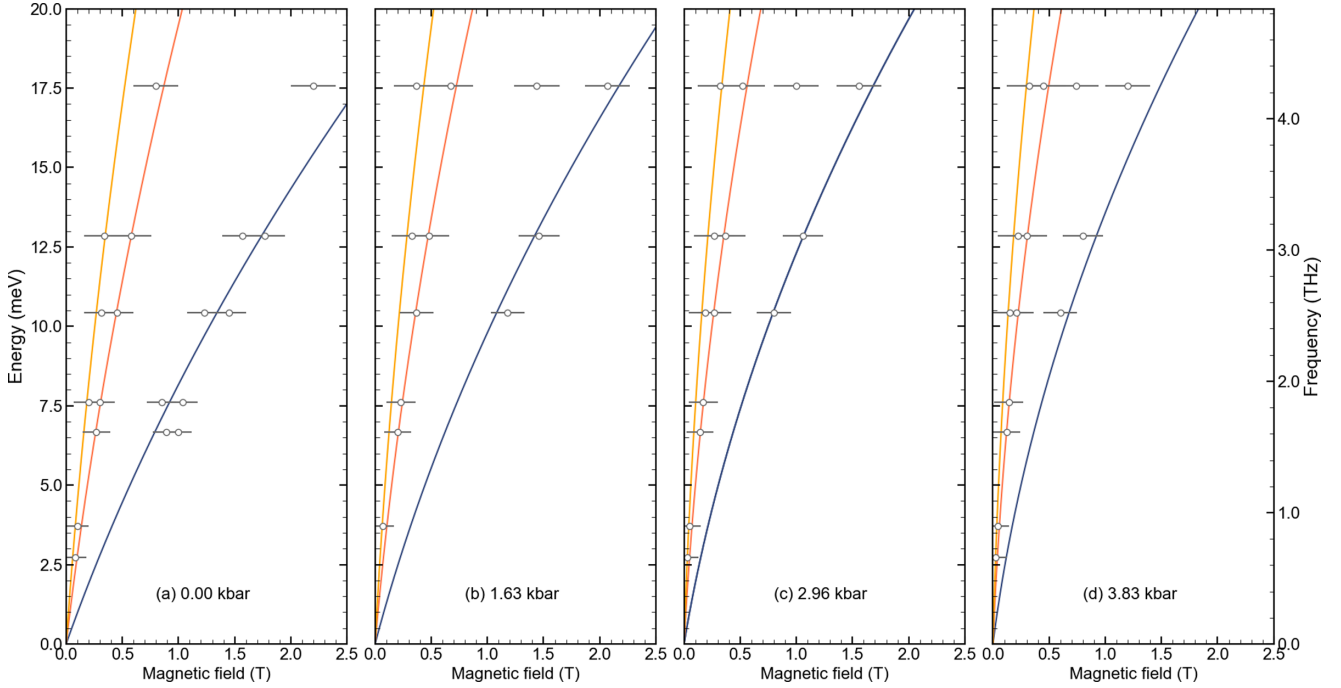
FIG. 2. Landau-level transitions as a function of magnetic field for sample A at four hydrostatic pressures: (a) $P = 0$ kbar, (b) $P = 1.63$ kbar, (c) $P = 2.96$ kbar, and (d) $P = 3.83$ kbar. Experimental data are represented by symbols. The solid lines represent the fits on the basis of the simplified Kane model [8] for three lines L_1 (blue), L_2 (orange), and L_3 (yellow) corresponding to $L_{1,2,\downarrow} - L_{0,n,\downarrow\uparrow}$, $L_{1,1,\uparrow} - L_{0,n,\downarrow\uparrow}$, and $L_{1,1,\downarrow} - L_{0,n,\downarrow\uparrow}$ LL transitions [see Eq. (2)], respectively.

determined by the extrapolation of the energy of optical transitions to zero magnetic field in sample C. To be able to extract the band-gap value of samples A and B, we use the negative pseudogap between the inverted Γ_6 conduction band and the Γ_8 heavy-hole band, thus extracting the band-gap value in a similar manner to the [8].

The energy limit of the Kane model is calculated by comparing the rest mass of the electrons with the heavy-hole mass. The gap energy at which the model is no longer valid is therefore of the order of 3 eV, that is to say, well beyond the gap energy of our samples.

Figure 2 respectively shows the detailed analysis performed for sample A, whereby absorption energy minima are identified (Fig. 1) and then plotted as a function of magnetic field in order to construct a Landau fan diagram. A simplified Kane model is then used to fit the data for three lines L_1, L_2, and L_3 corresponding to $L_{1,2,\downarrow} - L_{0,n,\downarrow\uparrow}$, $L_{1,1,\uparrow} - L_{0,n,\downarrow\uparrow}$, and $L_{1,1,\downarrow} - L_{0,n,\downarrow\uparrow}$ LL transitions, respectively (cf. Ref. [8]). One can see that not all the minima of magnetotransmission were taken into account in the data interpretation. Following Otteneder *et al.* [43], we attribute the origins of the observed resonances, the ones which were not used and occur around 1 T at 2.96 kbar at 17.5 meV, to the ionization of the impurities. This explanation also supports the various positions of these resonances between the different measured samples. An example of a Landau-level chart for sample A, at 0.0 kbar, with the main identified optical transitions L1, L2, and L3 is given in the Supplemental Material [39]. The LL energies at $p_z = 0$ are sufficient to describe the magneto-optical transmission spectra since the joint density of states is optimal for $p_z = 0$. During the analysis, we fitted only the rest mass

$\tilde{m}$, while the velocity was assumed to be $\tilde{c} = (E_P/3m_0)^{1/2} = 1.05 \times 10^6$ m/s, where m_0 is the free-electron mass and $E_P \approx 18.8$ eV is the Kane energy [42]. The velocity $\tilde{c}$ was previously demonstrated to be independent of temperature and Cd concentration [8]. The results for all samples are presented in Fig. 3 in the form of band gap $E_g = 2\tilde{m}\tilde{c}^2$ as a function of hydrostatic pressure. Detailed information on the fitting analysis for samples B and C is presented in the Supplemental Material [39]. It may be surprising not to see any Γ_6–Γ_8 transitions in sample B, as the gap falls within the experimental range. However, in sample B, the gap is closed and the band structure is inverted, such that the Γ_6 band lies below the
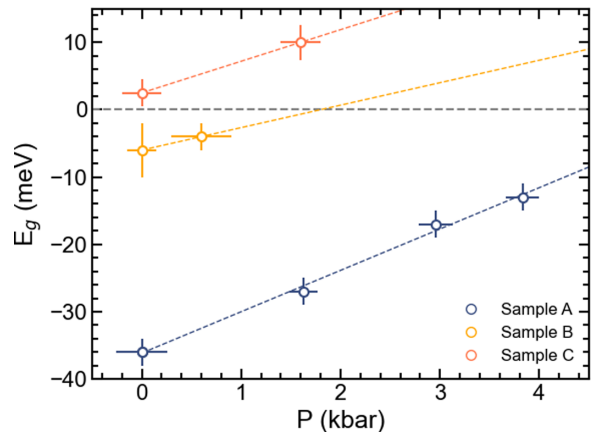

FIG. 3. Band gap $E_g = 2\tilde{m}\tilde{c}^2$ as a function of hydrostatic pressure extracted from the magnetic-field dependence of the LL transitions in all the samples under study.

Γ_8 heavy-hole band which has a high density of states. The Fermi level is therefore slightly above the Γ_8 heavy-hole band, which makes optical transitions from the Γ_6 conduction band to the Γ_8 heavy-hole band impossible since both bands are full. Transitions between the Γ_6 band and the Γ_8 conduction band are, however, possible, although not observed in our experiments. Indeed, their oscillator strength is weaker than the other optical transitions and their energy is higher.

IV. RESULTS AND DISCUSSION

Let us now determine the values of deformation potential $a_c - a_v$ from the experimental results shown in Fig. 3. The pressure dependence of the band gap $E_g = E_c - E_v$ in bulk crystal is defined by nonzero components of the strain tensor ϵ_{ij}:

$$E_g(P, T) = E_g^{(0)}(T) + (a_c - a_v)(\epsilon_{xx} + \epsilon_{yy} + \epsilon_{zz}), \quad (3)$$

where $E_g^{(0)}(T)$ is a temperature-dependent band gap in $Hg_{1-x}Cd_xTe$ in the absence of hydrostatic pressure [8,9], and the strain tensor components are determined on the basis of Murnaghan's equation of state [44]:

$$\epsilon_{xx} = \epsilon_{yy} = \epsilon_{zz} = \left(1 + P\frac{B_0'}{B_0(T)}\right)^{-1/3B_0'} - 1, \quad (4)$$

where B_0 is the temperature-dependent bulk modulus and $B_0' = \partial B_0 / \partial P$, which are determined by elastic constants $c_{ij}(P, T)$ as $B_0(T) = [c_{11}(T) + 2c_{12}(T)]/3$. Note that Eq. (4) is valid only if the elastic constants have linear dependence on P [45,46]:

$$c_{ij}(P, T) = c_{ij}^{(0)}(T) + P\frac{\partial c_{ij}}{\partial P}. \quad (5)$$

Here, $c_{ij}^{(0)}(T)$ are temperature-dependent elastic constants in $Hg_{1-x}Cd_xTe$ in the absence of hydrostatic pressure, while $\partial c_{ij}/\partial P$ is supposed to be independent of P and T. As in Ref. [36], $c_{ij}(P, T)$ and $\partial c_{ij}/\partial P$ are assumed to vary linearly with x in $Hg_{1-x}Cd_xTe$ alloy. For the calculation of B_0', we have used the values $\partial c_{ij}/\partial P$ reported in Refs. [45,46], resulting in 3.23 and 3.83 for CdTe and HgTe, respectively. The values of $c_{ij}^{(0)}(T)$ at given x are based on the experimental data for CdTe and HgTe, previously obtained from the measurements of ultrasonic wave velocities in bulk crystals [47].

Now, on the basis of Eqs. (3)–(5), we are able to convert band gap E_g at nonzero P into the deformation potential $a_c - a_v$. To determine the deformation potential at $P = 0$, we have used the Taylor's expansion of Eq. (4) resulting in quadratic dependence of $E_g(P)$ [36]. This allows the deformation potential to be expressed with a linear coefficient $\partial E_g/\partial P$ at zero pressure. The latter was calculated by using $E_g^{(0)}(T)$ at $P = 0$ and the value at the lowest available pressure for the given sample. Then, using a set of the $a_c - a_v$ values obtained from $E_g(P)$, we have calculated the mean and variance of the deformation potential for a given sample (see Table II).

Figure 4 summarizes the deformation potential values in $Hg_{1-x}Cd_xTe$ extracted from the analysis of far-infrared magneto-optical spectroscopy. The values for the samples under study are shown by blue open symbols. For comparison, we also added the values of $a_c - a_v$ recalculated from $\partial E_g/\partial P$
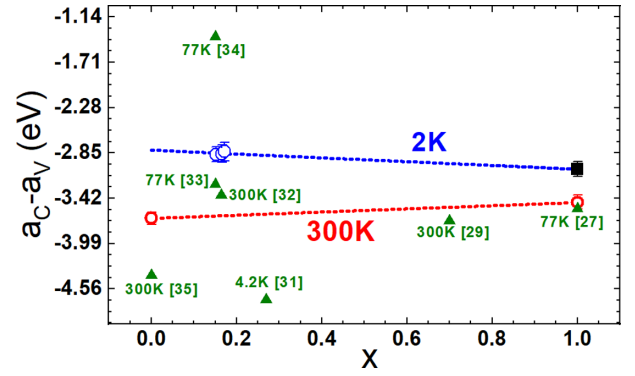

FIG. 4. Deformation potential $a_c - a_v$ in $Hg_{1-x}Cd_xTe$ at low and room temperatures. The red symbols and dotted line represent the values, and linear interpolation at 300 K recalculated from the results of Latussek *et al.* [36] based on the current values of $B_0(T)$ and B_0' used in this work. The black symbol corresponds to $a_c - a_v$ in CdTe recalculated from the low-temperature data of Dunstan *et al.* [28] (see Table I). Blue open symbols show the values obtained in this work (see Table II). The blue dotted line is the linear fitting of $a_c - a_v$ at 2 K. Green triangles represent the values of $a_c - a_v$ recalculated from $\partial E_g/\partial P$ provided in Refs. [27,29,31–35] (see Table I) by means of Eq. (6) and $B_0(T)$ used in this work.

in Table I by means of $B_0(T)$ at given temperature used in this work. For this, we have conditionally assumed that $\partial E_g/\partial P$ corresponds to the measurements at low hydrostatic pressures, which is actually not the case for some of the references. However, our assumption allows one to use a simple expression

$$\left.\frac{\partial E_g}{\partial P}\right|_{P=0} = -\frac{1}{B_0(T)}(a_c - a_v), \quad (6)$$

obtained from those of Eq. (3).

By applying the procedure described above to the low-temperature data of Dunstan *et al.* [28], we have also determined the deformation potential in CdTe, represented by the black symbol in Fig. 4. Then, assuming the linear variation of $a_c - a_v$ with Cd concentration [36], one can determine the deformation potential at 2 K in $Hg_{1-x}Cd_xTe$ for any values of x. Additionally, the red symbols in Fig. 4 represent the values of $a_c - a_v$ at 300 K recalculated from the results of Latussek *et al.* [36] based on the current values of $B_0(T)$ and B_0' used in this work. The linear fit of the deformation potential as a function of x gives $a_c - a_v \simeq -2.815 - 0.237x$ at 2 K, while the same procedure on the basis of the results of Latussek *et al.* [36] results in $a_c - a_v \simeq -3.675 + 0.208x$ at 300 K.

One can see the difference between low- and room-temperature deformation potentials, which indicates a temperature dependence of $a_c - a_v$ in $Hg_{1-x}Cd_xTe$. The origin of such a temperature dependence is not yet clear. Most likely, this is due to the features in the electron-phonon coupling inherent in $Hg_{1-x}Cd_xTe$ alloys. This specific coupling results in substantial temperature variation of the band gap $E_g^{(0)}(T)$ at any Cd concentration x [9] and should lead to the temperature dependence of hydrostatic deformation potentials as well.

V. CONCLUSION

In conclusion, we have performed pressure-dependent terahertz magneto-optical spectroscopy of $Hg_{1-x}Cd_xTe$ with x close to the semimetal-to-semiconductor topological phase transition. By analyzing the energies of interband optical transitions within the simplified Kane model, we have directly determined the rest mass of Kane fermions at different hydrostatic pressure. The pressure dependence of the rest mass allows obtaining the hydrostatic deformation potential $a_c - a_v$ at low temperature. By using the linear extrapolation between our values and those of Dunstan *et al.* [28], we have determined the deformation potential at different Cd concentrations x: $a_c - a_v \simeq -2.815 - 0.237x$ at 2 K. A comparison between our results and the values $a_c - a_v \simeq -3.675 + 0.208x$ at 300 K obtained by Latussek *et al.* [36] indicates the temperature dependence of the hydrostatic deformation potential in $Hg_{1-x}Cd_xTe$.

[1] A. Rogalski, HgCdTe infrared detector material: History, status and outlook, Rep. Prog. Phys. **68**, 2267 (2005).

[2] V. S. Varavin, S. A. Dvoretskii, N. N. Mikhailov, V. G. Remesnik, I. V. Sabinina, Y. G. Sidorov, V. A. Shvets, M. V. Yakushev, and A. V. Latyshev, Molecular beam epitaxy of CdHgTe: Current state and horizons, Optoelectron. Instrument. Proc. **56**, 456 (2020).

[3] A. M. Kadykov, J. Torres, S. S. Krishtopenko, C. Consejo, S. Ruffenach, M. Marcinkiewicz, D. But, W. Knap, S. V. Morozov, V. I. Gavrilenko, N. N. Mikhailov, S. A. Dvoretsky, and F. Teppe, Terahertz imaging of Landau levels in HgTe-based topological insulators, Appl. Phys. Lett. **108**, 262102 (2016).

[4] S. Ruffenach, A. Kadykov, V. V. Rumyantsev, J. Torres, D. Coquillat, D. But, S. S. Krishtopenko, C. Consejo, W. Knap, S. Winnerl, M. Helm, M. A. Fadeev, N. N. Mikhailov, S. A. Dvoretskii, V. I. Gavrilenko, S. V. Morozov, and F. Teppe, HgCdTe-based heterostructures for terahertz photonics, APL Mater. **5**, 035503 (2017).

[5] S. V. Morozov, V. V. Rumyantsev, M. A. Fadeev, M. S. Zholudev, K. E. Kudryavtsev, A. V. Antonov, A. M. Kadykov, A. A. Dubinov, N. N. Mikhailov, S. A. Dvoretsky, and V. I. Gavrilenko, Stimulated emission from (HgCdTe) quantum well heterostructures at wavelengths up to 19.5 μm, Appl. Phys. Lett. **111**, 192101 (2017).

[6] K. E. Kudryavtsev, V. V. Rumyantsev, V. Y. Aleshkin, A. A. Dubinov, V. V. Utochkin, M. A. Fadeev, N. N. Mikhailov, G. Alymov, D. Svintsov, V. I. Gavrilenko, and S. V. Morozov, Temperature limitations for stimulated emission in 3-4μm range due to threshold and non-threshold Auger recombination in HgTe/CdHgTe quantum wells, Appl. Phys. Lett. **117**, 083103 (2020).

[7] V. V. Utochkin, K. E. Kudryavtsev, M. A. Fadeev, A. A. Razova, D. S. Bykov, V. Y. Aleshkin, A. A. Dubinov, N. N. Mikhailov, S. A. Dvoretsky, V. V. Rumyantsev, V. I. Gavrilenko, and S. V. Morozov, Mid-IR stimulated emission in Hg(Cd)Te/CdHgTe quantum well structures up to 200 K due to suppressed Auger recombination, Laser Phys. **31**, 015801 (2021).

[8] F. Teppe, M. Marcinkiewicz, S. S. Krishtopenko, S. Ruffenach, C. Consejo, A. M. Kadykov, W. Desrat, D. But, W. Knap, J. Ludwig, S. Moon, D. Smirnov, M. Orlita, Z. Jiang, S. V.

Morozov, V. Gavrilenko, N. N. Mikhailov, and S. A. Dvoretskii, Temperature-driven massless Kane fermions in HgCdTe crystals, Nat. Commun. **7**, 12576 (2016).

[9] J. P. Laurenti, J. Camassel, A. Bouhemadou, B. Toulouse, R. Legros, and A. Lusson, Temperature dependence of the fundamental absorption edge of mercury cadmium telluride, J. Appl. Phys. **67**, 6454 (1990).

[10] L. Fu and C. L. Kane, Topological insulators with inversion symmetry, Phys. Rev. B **76**, 045302 (2007).

[11] C. Brüne, C. X. Liu, E. G. Novik, E. M. Hankiewicz, H. Buhmann, Y. L. Chen, X. L. Qi, Z. X. Shen, S. C. Zhang, and L. W. Molenkamp, Quantum Hall Effect from the Topological Surface States of Strained Bulk HgTe, Phys. Rev. Lett. **106**, 126803 (2011).

[12] J. Ruan, S.-K. Jian, H. Yao, H. Zhang, S.-C. Zhang, and D. Xing, Symmetry-protected ideal Weyl semimetal in HgTe-class materials, Nat. Commun. **7**, 11136 (2016).

[13] D. M. Mahler, J.-B. Mayer, P. Leubner, L. Lunczer, D. Di Sante, G. Sangiovanni, R. Thomale, E. M. Hankiewicz, H. Buhmann, C. Gould, and L. W. Molenkamp, Interplay of Dirac Nodes and Volkov-Pankratov Surface States in Compressively Strained HgTe, Phys. Rev. X **9**, 031034 (2019).

[14] D. A. Kozlov, Z. D. Kvon, E. B. Olshanetsky, N. N. Mikhailov, S. A. Dvoretsky, and D. Weiss, Transport Properties of a 3D Topological Insulator based on a Strained High-Mobility HgTe Film, Phys. Rev. Lett. **112**, 196801 (2014).

[15] B. A. Bernevig, T. L. Hughes, and S.-C. Zhang, Quantum spin Hall effect and topological phase transition in HgTe quantum wells, Science **314**, 1757 (2006).

[16] M. König, S. Wiedmann, C. Brüne, A. Roth, H. Buhmann, L. W. Molenkamp, X.-L. Qi, and S.-C. Zhang, Quantum spin Hall insulator state in HgTe quantum wells, Science **318**, 766 (2007).

[17] S. S. Krishtopenko, W. Knap, and F. Teppe, Phase transitions in two tunnel-coupled HgTe quantum wells: Bilayer graphene analogy and beyond, Sci. Rep. **6**, 30755 (2016).

[18] E. B. Olshanetsky, Z. D. Kvon, G. M. Gusev, A. D. Levin, O. E. Raichev, N. N. Mikhailov, and S. A. Dvoretsky, Persistence of a Two-Dimensional Topological Insulator State in Wide HgTe Quantum Wells, Phys. Rev. Lett. **114**, 126802 (2015).

[19] S. S. Krishtopenko, I. Yahniuk, D. B. But, V. I. Gavrilenko, W. Knap, and F. Teppe, Pressure- and temperature-driven phase transitions in HgTe quantum wells, Phys. Rev. B **94**, 245402 (2016).

[20] M. Marcinkiewicz, S. Ruffenach, S. S. Krishtopenko, A. M. Kadykov, C. Consejo, D. B. But, W. Desrat, W. Knap, J. Torres, A. V. Ikonnikov, K. E. Spirin, S. V. Morozov, V. I. Gavrilenko, N. N. Mikhailov, S. A. Dvoretskii, and F. Teppe, Temperature-driven single-valley Dirac fermions in HgTe quantum wells, Phys. Rev. B **96**, 035405 (2017).

[21] A. M. Kadykov, S. S. Krishtopenko, B. Jouault, W. Desrat, W. Knap, S. Ruffenach, C. Consejo, J. Torres, S. V. Morozov, N. N. Mikhailov, S. A. Dvoretskii, and F. Teppe, Temperature-Induced Topological Phase Transition in HgTe Quantum Wells, Phys. Rev. Lett. **120**, 086401 (2018).

[22] Z. D. Kvon, D. A. Kozlov, E. B. Olshanetsky, G. M. Gusev, N. N. Mikhailov, and S. A. Dvoretsky, Topological insulators based on HgTe, Phys. Usp. **63**, 629 (2020).

[23] G. A. Babonas, R. A. Bendoryus, and A. Yu. Shileika, Photoluminescence of CdTe under hydrostatic pressure, Sov. Phys. Semicond. **5**, 392 (1971).

[24] J. Mei and V. Lemos, Photoluminescence on CdSe and CdTe under hydrostatic pressure, Solid State Commun. **52**, 785 (1984).

[25] W. Shan, S. Shen, and H. Zhu, Pressure dependence of the absorption edge for $Cd_{1-x}Mn_xTe$, Solid State Commun. **55**, 475 (1985).

[26] J. González, F. Pérez, E. Moya, and J. Chervin, Hydrostatic pressure dependence of the energy gaps of CdTe in the zinc-blende and rocksalt phases, J. Phys. Chem. Solids **56**, 335 (1995).

[27] H. Cheong, J. Burnett, and W. Paul, Photoluminescence of CdTe under hydrostatic pressure, Solid State Commun. **77**, 565 (1991).

[28] D. J. Dunstan, B. Gil, and K. P. Homewood, Hydrostatic and uniaxial pressure coefficients of CdTe, Phys. Rev. B **38**, 7862 (1988).

[29] S. Jiang, S. C. Shen, D. Li, Y. Q. Ju, H. Zhu, and J. Schilz, Pressure dependence of energy gap for $Cd_{0.7}Hg_{0.3}Te$, Appl. Phys. Lett. **60**, 3171 (1992).

[30] C. Verié, Sur la structure de bandes des alliages HgTe-CdTe I. Mesures électriques, Phys. Status Solidi B **17**, 889 (1966).

[31] J. C. Gonthier, A. Raymond, J. L. Robert, R. Triboulet, and J. P. Faurie, Characterisation under hydrostatic pressure of narrow-gap $Hg_{1-x}Cd_xTe$ and $Hg_{1-x}Zn_xTe$, Semicond. Sci. Technol. **5**, S217 (1990).

[32] M. Carvalho, C. Fau, and M. Averous, First order phase transition of Hall coefficient versus magnetic field, under hydrostatic pressure due to freeze-out on acceptor state in $Hg_{0.836}Cd_{0.164}Te$, in *Physics of Narrow Gap Semiconductors*, edited by E. Gornik, H. Heinrich, and L. Palmetshofer (Springer, Berlin, Heidelberg, 1982), pp. 430–434.

[33] C. T. Elliott, J. Melngailis, T. C. Harman, J. A. Kafalas, and W. C. Kernan, Pressure dependence of the carrier concentrations in *p*-type alloys of $Hg_{1-x}Cd_xTe$ at 4.2 and 77 K, Phys. Rev. B **5**, 2985 (1972).

[34] C. Fau, J. F. Dame, M. de Carvalho, J. Calas, M. Averous, and B. A. Lombos, Three-band model applied to narrow-gap HgCdTe, Phys. Status Solidi B **125**, 831 (1984).

[35] J. Stankiewicz and W. Giriat, Galvanomagnetic properties of pure HgTe under high hydrostatic pressure, Phys. Rev. B **13**, 665 (1976).

[36] V. Latussek, C. R. Becker, G. Landwehr, R. Bini, and L. Ulivi, Deformation potentials of the semimetal HgTe, Phys. Rev. B **71**, 125305 (2005).

[37] D. Yavorskiy (private communication).

[38] Y. Sidorov, A. Anciferov, V. Varavin, S. Dvoretsky, N. Mikhailov, M. Yakushev, I. Sabinina, V. Remesnik, D. Ikusov, I. Uzhakov, G. Sidorov, V. Kuzmin, S. Rihlicky, V. Shvets, A. Mardezov, E. Spesivcev, A. Gutakovskii, and A. Latyshev, Molecular beam epitaxy of $Cd_xHg_{1-x}Te$, in *Advances in Semiconductor Nanostructures*, edited by A. V. Latyshev, A. V. Dvurechenskii, and A. L. Aseev (Elsevier, New York, 2017), Chap. 12, pp. 297–323.

[39] See Supplemental Material at http://link.aps.org/supplemental/10.1103/PhysRevB.106.195202 for magnetotransmission spectra and their analysis for samples A, B, and C.

[40] Institute of High Pressure Physics, Polish Academy of Sciences, Warsaw, Unipress equipment, https://unipress.waw.pl/.

[41] S. S. Krishtopenko, M. Antezza, and F. Teppe, Hybridization of topological surface states with a flat band, J. Phys.: Condens. Matter **32**, 165501 (2020).

[42] M. Orlita, D. M. Basko, M. S. Zholudev, F. Teppe, W. Knap, V. I. Gavrilenko, N. N. Mikhailov, S. A. Dvoretskii, P. Neugebauer, C. Faugeras, A.-L. Barra, G. Martinez, and M. Potemski, Observation of three-dimensional massless Kane fermions in a zinc-blende crystal, Nat. Phys. **10**, 233 (2014).

[43] M. Otteneder, D. Sacré, I. Yahniuk, G. V. Budkin, K. Diendorfer, D. A. Kozlov, I. A. Dmitriev, N. N. Mikhailov, S. A. Dvoretsky, V. V. Bel'kov, W. Knap, and S. D. Ganichev, Terahertz magnetospectroscopy of cyclotron resonances from topological surface states in thick films of $Cd_xHg_{1-x}Te$, Phys. Status Solidi B **258**, 2000023 (2021).

[44] M. D. Frogley, J. L. Sly, and D. J. Dunstan, Pressure dependence of the direct band gap in tetrahedral semiconductors, Phys. Rev. B **58**, 12579 (1998).

[45] E. Deligoz, K. Colakoglu, and Y. Ciftci, Elastic, electronic, and lattice dynamical properties of CdS, CdSe, and CdTe, Phys. B: Condens. Matter **373**, 124 (2006).

[46] S. Adachi, in *Properties of Group-IV, III-V and II-VI Semiconductors*, edited by P. Capper, S. Kasap, and A. Willoughby (Wiley, New York, 2005).

[47] *Mercury Cadmium Telluride: Growth, Properties and Applications*, edited by P. Capper and J. Garland (Wiley, New York, 2011).